Global NEST Journal, Vol 25, No 9, pp 167-175

Integrated disaster risk management for flood detection on remote sensing images using deep learning techniques

Arun Mozhi Selvi Sundarapandi.[1], Deepa R.[2], Subhashini P.[3] and Venkatesh Jayaraman[4]

[1]Department of Computer Science and Engineering, Holycross Engineering College, Thoothukudi - 628851, Tamil Nadu, India

[2]Department of Computing Technologies, School of Computing, College of Engineering and Technology, SRM Institute of Science and Technology, SRM Nagar, Kattankulathur, Chennai, Tamil Nadu, India

[3]Department of Information Technology, Vel Tech Multi Tech Dr. Rangarajan Dr. Sakunthala Engineering College, Chennai - 600062, Tamil Nadu, India

[4]Department of Computer Science and Engineering, Chennai Institute of Technology, Chennai - 600069, Tamil Nadu, India

Received: 22/08/2023, Accepted: 14/09/2023, Available online: 19/09/2023

*to whom all correspondence should be addressed: e-mail: arunmozhiselvisundarapandi@gmail.com

https://doi.org/10.30955/gnj.005317

Graphical abstract

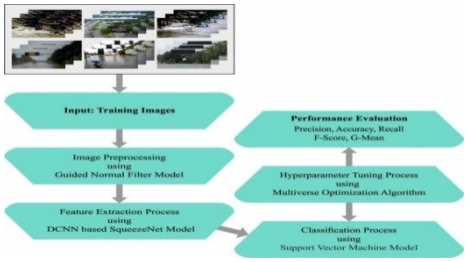

Abstract

Floods are one of the leading causes of damage, prompting mortality and substantial destruction to the structure and total economy of the affected nations. Remote sensing, satellite imagery, global positioning system, and geographic information system (GIS) are widely employed for flood identification to examine flood-related losses. Recently, accurate and automated flood detection models using remote sensing images have become effective for flood disaster management, risk manager, infrastructure planning, disaster rescue management, etc. Computer vision and deep learning (DL) models provide prompt and rapid flood detection in remote sensing images. In this aspect, this paper presents a multiverse optimization with a deep transfer learning-enabled flood detection (MVODTL-FD) technique for disaster risk management. In the proposed MVODTL-FD technique, remote sensing images are investigated for the effectual detection of floods. To accomplish this, the presented MVODTL-FD technique applies a guided normal filter (GNF) based image preprocessing approach to eliminate the noise. In addition, the proposed MVODTL-FD technique uses a deep convolutional neural network-based Squeeze Net model for feature extraction, and the hyperparameter process is performed using the MVO algorithm. At last, the flood detection process is performed using support vector machine (SVM) classification. For establishing the improved version of the MVODTL-FD method, a wide-ranging experimental analysis is performed. The MVODTL-FD model is rated higher in the comparative analysis than other DL models.

Keywords: Remote sensing, disaster risk management, flood detection, deep learning

1. Introduction

Almost 80% of the world's population is expected to live in urban regions, meaning one-third of the economic losses caused by natural disasters globally are caused by flood damage. Floods have accounted for 43% of all known disasters worldwide over the last 20 years. Flooding events are estimated to become more frequent and prevalent due to climate change, including extreme heavy precipitation events, quick spring snow melt, and severe storm surges. Jean R. *et al*., (2020) described the flooding has a variety of negative consequences such as the loss of human life, risks of road closures, erosion and landslides, threats to aquatic species, and water contamination posing health problems. This unprecedented gathering of people and infrastructure was shifting the emphasis of disaster risk management (DRM) research work toward cities. Santhanaraj R.K. *et al*., (2023) explained the ability of a system to recover, resist, absorb, and accommodate the impacts of a hazard in an efficient and timely manner is called resilience, and it is becoming crucial to reduce disaster risk. Li X. *et al*., (2020) was developed, the resilience even includes postevent processes that permit communities to learn, reorganize, and change responding to an event. Later, improving the resilience of the community to natural hazards indicates enhancing its ability to anticipate menaces, reducing its complete vulnerability, and allowing the community to recovering from adverse effects when they occur.

Tanim A.H. *et al*., (2022) implement the Remote sensing (RS) rapid tool to monitor larger areas and is vital for gaining geospatial data, which creates the base for risk

management and assessment. Jain P. *et al*., (2020) elaborate the broadly utilized for several facets of the DRM, extending from vulnerability to rapid damage valuations, for various areas ranging from coastal environments to complicated urban settings, and for disasters as different as cyclones or landslides. Duhayyim M.A. *et al*., (2023) developed the RS to provide information regarding the forthcoming disaster and event obstacles, along with an extraction of the flood region's features. Munawar H.S. *et al*., (2022) execute the new disaster management becomes a multi-faceted and strategic process for response, mitigation, recovery, and preparedness for protecting the critical intrastate and vulnerable communities in several disasters. However, every disaster was connected to human beings coping with their significance. Chawan A.C. *et al*., (2020) defined failure and success relying on the implementation and planning of effectual disaster management observers. Tamilvizhi *et al*., (2022) implementing the disaster management deep learning (DL) becomes a significant force multiplier with the capability of protecting property and people in the disaster of tragedy and is surely the future of disaster management. AI can forecast floods before events arise. Compared to standard approaches, AI uses real-time observed data to forecast flooding and can prevent 30 to 50% of damage because flood warnings are broadcast in milliseconds. To accurately predict flooding, AI uses two main models: a hydrology model to estimate river levels of water and an invasion model to prevent property damage and fatalities.

Shehata M. *et al*., (2021) develop, the disaster response planning can be suggestively influenced by ecology, morphology, weather conditions, the machinery's available resources, and other factors. It can be suggested to utilize operations research and management science criteria for enhancing resilience in emergency relief whereas concerning the effect of relief resource allotment over the population. Rambour C. *et al*., (2020) showed numerous studies assessing the use of DL. The crisis response condition in other nations differed from India. Thus, there comes a necessity to prioritize and find the data required to compel crises in natural disasters. The right way to reduce the effect of catastrophe is readiness, vulnerability, prevention, and resilience in disaster management. Shafique A. *et al*., (2022) explained that the AI and geographic information systems (GIS) were essential tools utilized by several researchers for plotting the spatial distribution of flood hazards and vulnerability to flooding. The GIS serves as a facilitator that manages, inputs, incorporates, delivers, and stores spatial information for real-time decision-making and strategic planning for effective and timely hazard readiness and flood disaster management.

This paper presents a multiverse optimization with a deep transfer learning-enabled flood detection (MVODTL-FD) technique for disaster risk management. The demonstrated MVODTL-FD technique applies a guided normal filter (GNF) based image preprocessing approach to eliminate the noise. In addition, the demonstrated MVODTL-FD technique uses a deep convolutional neural network-based Squeeze Net model for feature extraction. For demonstrating the improved version of the MVODTL-FD model, an extensive experimental analysis is carried out. The comparison analysis noted that the MVODTL-FD model outperformed other DL models. The gap in the current work is the overall accuracy and the process results must be improved. The image quality using datasets is not satisfactory and compared to the MVODTL-FD approach, which employs a deep convolutional neural network-based Squeeze Net model. The Objectives of the proposed work,

- To develope a new MVODTL-FD technique for the flood detection process through remote sensing images.
- To eliminate the noise through GNF based image pre-processing approach
- To compare the study report of MVODTL-FD model over other models.

The remainder of the paper is organized as follows, Section 2 analysis the related works involved in Flood Detection techniques. Section 3 describes the Proposed MVODTL-FD technique. Section 4 then analyses the Results and discussion, including a performance comparison with alternative methodologies. Finally, Section 5 concludes the critical results of the proposed research.

2. Related works

Surendran R. *et al*., (2023) suggested today's AI systems and geospatial technology were advanced and can be effective in crises. Khan A.A. *et al*. (2022) address these problems by utilizing an innovative CNN-related structure. The presented network includes either spatial or spectral data that compiles two subnetworks, which are spectral-CNN and spatial-CNN. Furthermore, a multiscale spatial CNN structure was proposed using various kernels to make the features more robust. Li W. *et al*., (2019) inspected a DL-related classification technique for RSI, mainly for high spatial resolution remote sensing (HSRRS) images having multiscene classes and various changes. To be specific, the author concerns with the 4 DNNs, which are CNN and CapsNet, similar methods with diverse training rounding related to CNN (SMDTR-CNN), and the same approach with various trained rounding related to CapsNet (SMDTR-CapsNet) to help develop the respective classification techniques in urban built-up areas. Munawar H.S. *et al*., (2021) introduce a new approach by combining ML and image processing for detecting flood-affected regions through a set of images. The three-step method offered in this work depends on landmark detection from pictures, training of an ML technique, and categorizing images from an area into non-flooded and flooded. Bhadra T. *et al*., (2020) devised flood detection in the real world by using SAR data and multispectral images utilizing DL method and CNN. CNN has revealed outstanding performance in image-based tasks such as feature extraction, classification, and segmentation. Currently, the DL methods are utilized widely in RSI because of their high

resolution and the former's broad computational capability.

Hashemi-Beni L. *et al*., (2021) solved the problem by presenting a combined CNN and region growing (RG) technique for mapping underneath vegetation and visible flooded areas. The CNN-related classification can be utilized for extracting flooded regions through optical images. At the same time, the RG technique can be enforced for predicting the extent of floods underneath vegetation that are invisible from images using the digital elevation method. Katiyar V. *et al*., (2021) utilized this dataset for improving flood detection with the help of segmentation structures, namely, UNet and SegNet networks. Moreover, this study offered a deep understanding of which group of polarized band combinations was appropriate for distinguishing permanent water along with flooded regions from the SAR imagery. The complete performance of the method with a variety of bands and various types of labels for detecting all surface water areas is measured. Ahmad K *et al*. (2019) solved the issue of flood aftermath detection and flood classification related to both satellite images and social media. But still, automatic recognition of disasters like floods becomes complicated. The concentration is on recognizing roads or passable routes during floods. The studies were differentiating and detecting non-passable and good roads using imagery from 2 complementary information sources and catching images offering evidence for road possibility. As an initial challenge, the author mostly depends on the object and scene-level features derived by many deep methods pretrained on ImageNet and Place data.

Li J. *et al*., (2022) devised a novel, precise water-extracting structure related to NDWI of multispectral images and unsupervised DL. Binarized NDWI imagery is utilized for identifying influential water bodies, and DL training can be executed by these labels and pseudo samples. This procedure will realize the change from unlabeled to noisy label learning. Firstly, the authors devised a simple and fast binarization method for segmenting several natural water bodies in NDWI imagery. Next, the group of water confidence valuation rules has been built from the four aspects of the range, shape spectrum, and aggregation. Surendran R. *et al*., (2023) calculate the hyperparameter tuning process is performed using the MVO algorithm. At last, the flood detection process is completed by utilizing of support vector machine (SVM) technique.

3. The proposed model

In this research work, a proposed MVODTL-FD system was established for the flood detection process. In the proposed MVODTL-FD technique, remote sensing images are investigated for the effectual detection of floods. To accomplish this, the proposed MVODTL-FD technique utilized GNF based image preprocessing approach to get rid of the noise. In addition, the proposed MVODTL-FD technique uses a deep convolutional neural network-based SqueezeNet model for feature extraction, and the hyperparameter tuning process is performed using the MVO algorithm. At last, the flood detection process is performed using the SVM classifier. Figure 1 demonstrates the block diagram of the MVODTL-FD algorithm.

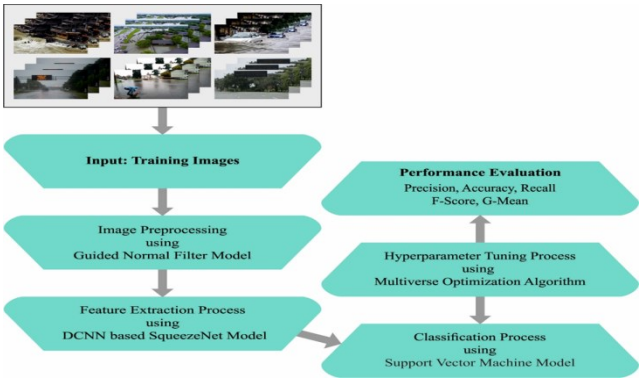

Figure 1. Block diagram of MVODTL-FD approach

3.1. Image pre-processing

Firstly, the presented MVODTL-FD technique utilized GNF based image preprocessing approach to eliminate the noise. The GNF approach is an adapted one-stage algorithm. The procedure through which the noise removal process employs the GNF model is denoted by (update normal + (update vertices) $^{viter})^{iter}$, and it is evaluated using the following.

$$\tilde{n}_i = \frac{1}{K_i} \times \sum_{f_j \in \Omega_i} A_j W_c \left(\| c(f_i) - c(f_j) \|, \sigma_c \right) W_s \left(\| g_i - g_j \|, \sigma_s \right) n_j \quad (1)$$

In Eq. (1), g_i indicates a guided normal vector of f_i and is intended to be vital for noise. The chosen patch has the average direction, and the selective patch was utilized as the normal guidance g_i for the face f_i. The GNF preserving feature is superior to BNF since g_i is vital for the noise than n_i. Remarkably, Ω_i is employed in GNF while facing in Φ_i is assumed in BNF.

3.2. Feature extraction

The SqueezeNet model, based on deep convolutional neural networks, is used by the reported MVODTL-FD technique to extract features. While requiring fifty times as many variables as AlexNet, SqueezeNet is a convolutional network that performs better derived by Shaiba H. (2022). Among the 15 layers that make up SqueezeNet are one global average pooling layer, one softmax output layer, two convolution layers, three max-pooling levels, and eight fire layers. The training parameter is selected and fed into a pretrained SqueezeNet model, which learns from the adapted data. It was implemented by Mirjalili S (2016). The DCNN SqueezeNet contains eighteen layers. The SqueezeNet is a design which that guarantees better efficacy while handling a constrained amount of network parameters. SqueezeNet initiates with a single convolutional layer (conv1), the following eight Fire modules (fire2–9), and the last another convolutional layer. Afterward, in conv10, fire8, fire4, and conv1 layers, SqueezeNet implements max-pooling with a stride of 2. The accessible field of filter size can be denoted as K × K notation in SqueezeNet design, while the feature map length is signified as l and the stride size is signified as s. The RGB channels and

227×227 size of the network input are present. The image is then used to specialise in information using convolution and max pooling. Zhang X. *et al*., (2021) used 3×3 kernels, the convolutional layer connecting the input volume's weight and constraint regions. The actual part of each convolutional layer's argument is carried out through element-by-element activation. Fire layers with squeeze and extended stages are used by SqueezeNet in between the convolution layers. Equal input and output tensor scales apply to the fire. 1×1 filters are used during the squeeze phase, while 3×3 and 1×1 filters are used during the expansion phase. First, the input tensors H, W, and C are squeezed with C/4 of the input tensor channels' worth of convolutions. The data moves to extension in the first step, where its depth is raised to C/2 of the resulting tensor depth. The ReLu units support the squeezing and expanding processes. The devised approach increases the depth while maintaining the same feature size as the squeeze scheme reduces it. The expanded results are then stacked in the input tensor's depth dimension using the concatenated method similar to Akshaya K.G. *et al*., (2023).

In this study, the hyperparameter tuning process is performed using the MVO algorithm, Karthikeyan B. *et al*., (2023) developed the MVO as a nature-based model. This process is the primary motivation for the proposed concept of multiverse in astrophysics. According to the MVO, the extended bang procedure has different universes, whereas worm, white, and black holes interconnect those universes. The researchers claimed that the matter of the MVO moves in a universe to others through black or white holes such that white and black holes emit and attract correspondingly. Wormholes interconnect two sides of the universe. The key terms of these theories are given in the following: every universe is a solution, whereas all solutions are encompassed by the sequence of generations, iterations, or objects utilized to determine the time, and the inflation rate is used to determine the value of all things in a specific universe. In such theories, the solution is equivalent to a galaxy with different wormholes, or white spots or black holes. For improving the values of objects, white holes are considered highly possible in a specific solution that shows the highest value. At the same time, black holes are highly potentially designed in objects with the worst deal that creates the communication of importance of the variable with a satisfactory solution. This improves the probability of weaker solutions that are sequentially transformed into a better mean value of each key.

$$x_i^{'} = \begin{cases} x_k^{'} \; r_1 < NI(U_i) \\ x_i^{'} \; r_1 \geq NI(U_i) \end{cases} \tag{2}$$

In Eq. (2), X_i^j characterizes the jth object of the ith universe, r_1 shows the random value in a predetermined spectrum range within [0, 1], NI (U_i) as equivalent to the normalizing inflation rate of the ith universe, and X_k^j characterizes the jth objects of the kth universe.

In Eq. (3), X_j indicates the jth centroid of the finest universe, UB signifies the upper bound, LB equals the Wormhole Existence Probability (WEP), minimal determined, and Traveling Distance Rate (TDR) are coefficient, r_2, r_3, and r_4 represents random numbers within zero and one.

$$x_i^{'} = \begin{cases} x_j + TDR \times ((Ub_b - Lb_b) \times r_4 \times Lb_b) \; r_3 < 0.5 \,|\, r_2 < WEP \\ x_j - TDR \times ((Ub_b - Lb_b) \times r_4 \times Lb_b) \; r_3 \geq 0.5 \,|\, r_2 < WEP \\ x_i^{'} \; r_2 \geq WEP \end{cases} \tag{3}$$

As well, the process of MVO signifies the best solution to apply and optimize to impact other solutions. During this study, the author claimed that wormholes are established in each universe. Then, it improves the probability of having access to the best solution, and maintaining the best solution is accomplished by the optimized approach. The precondition of resolving the aforementioned equation above is replacing the parameters among different solutions. It is notable that if the equation is employed in the same pattern (exploitative or exploratory) yield the same outcomes. The MVO comprises the subsequent process to suitably focus on different ways in the optimization pattern in Eq. (4).

$$WEP = \text{Min} + Iteration \times \left(\frac{\text{Max} - \text{Min}}{L} \right) \tag{4}$$

$$TDR = 1 - \frac{Iteration^{1/p}}{L^{1/p}} \tag{5}$$

From Eq. (5), p indicates the exploitation components. Two kinds of adaptive parameters are presented in MVO: TDR and WEP. To increase the accuracy of exploitation or local in defining the optimal solution, TDR must be improved in different iterations. WEP rises according to the frequency of iteration to improve exploitation. Therefore, MVO is regarded as a revolutionary model for exchanging matters. It results in an unexpected change in the universe, which enhances the exploration and keeps the universe's diversity when implementing the iteration. Afterward, recognizing the better universe, all universes take a sequence of parameters in random methodology. This technique shows the mutation, a revolutionary model. Sequentially, the mutation operation leads to small alternations for better solutions and exploitation. Elitism is an extreme operator used for maintaining a better solution accomplished by an optimization technique. The elitism accomplishes by discovering a better universe.

A fitness function (FF) is enhanced using the MVO system to achieve better classifier results. It specifies a positive number to represent the candidate outcomes that performed the best. In this instance, it is assumed that FF is given Eq in order to minimize the classifier error rate (6).

$$\begin{aligned} fitness(x_i) &= ClassifierErrorRate(x_i) \\ &= \frac{number\ of\ misclassified\ samples}{Total\ number\ of\ samples} * 100 \end{aligned} \tag{6}$$

3.3. Flood detection using SVM

Finally, the flood detection process is performed using the SVM classifier. A multiclass SVM was utilized as the classification mechanism. SVM functions on the standard of disaster risk management. It is better suitable for

classification tasks once the sampling size is not that big. The main idea is to discover the optimum hyperplane that distinguishes the trained dataset into two double categories by increasing the margin. In a multiclass classifier problem, the dataset except the targeted one is integrated for creating dual classifier situations. Figure 2 depicts the hyperplane of SVM. The dataset point positioned nearby the imaginary line is called a support vector.

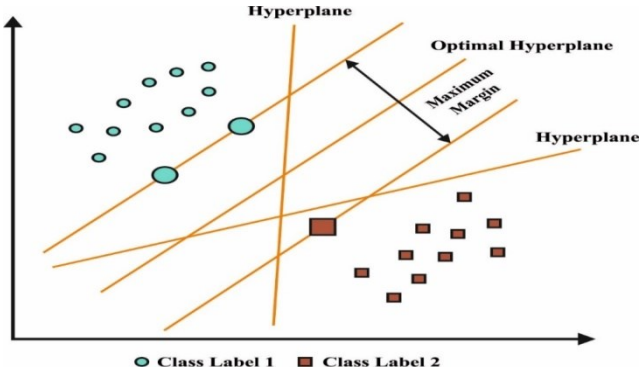

Figure 2. Hyperplane SVM

For the provided set of information(u_1,v_1), (u_2,v_2), …, (u_n,v_m), $u_i \in R^n$ are taken into account as input, whereby u and v represent corresponding data points of support vector, and $v_i \in (-1, +1)$ indicates the output for every u_i . It is expressed in Eq. (7).

$$(w \cdot u) + b = 0, \tag{7}$$

Eq. (8), w indicates a vector with dimension N, and b shows a scalar quantity. In general form, the equation of hyperplane for $v_i = 1$ and $v_i = -1$ is indicated below Eq. (9).

$$(w \cdot u_i) + b \geq 1, \tag{8}$$

$$(w \cdot u_i) + b \leq 1. \tag{9}$$

By a positive margin,

$$(w^T \cdot u_2) + b = +1. \tag{10}$$

For negative margin,

$$(w^T \cdot u_1) + b = -1. \tag{11}$$

By deducting Eq. (11) from Eq. (10), obtain the maximal margin by Eq. (12).

$$w^T (u_2 - u_1) = 2, \tag{12}$$

$$\frac{w^T}{\| w \|} \cdot (u_2 - u_1) = \frac{2}{\| w \|}. \tag{13}$$

This is the enhanced function that should be increased in Eq. (13).

Error optimization: For novel testing dataset V_i, one gets

$$v_i * (w^T \cdot u_i) + b_i \geq 1. \tag{14}$$

Once the abovementioned condition is not fulfilled in Eq. (14), it denotes a case of misclassification. In such cases, it is necessary to add the error term for calculating w and b.

$$(w^*, b^*) = \min \frac{\| w \|}{2} + C_i \sum_{i=1}^{n} \varepsilon_{i,} \tag{15}$$

In Eq. (15), C indicates the error penalty, and ε denotes the slack parameter.

4. Results and discussion

The flood detection results of the MVODTL-FD model are tested using a dataset comprising 400 samples. A few sample images are portrayed in Figure 3.

Figure 3. Sample images

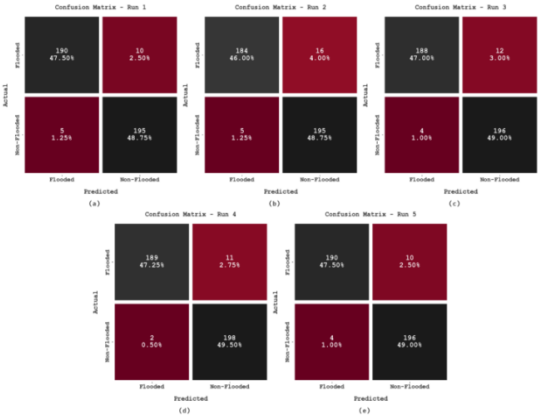

Figure 4. Confusion matrices of MVODTL-FD approach (a) Run1, (b) Run2, (c) Run3, (d) Run4, and (e) Run5

The flood detection results of the MVODTL-FD model are represented in the form of a confusion matrix in Figure 4. On run-1, the MVODTL-FD model has categorized 190 samples into flooded classes and 195 pieces into non-flooded types. Concurrently, in run-2, the MVODTL-FD approach has categorized 184 pieces into flooded types and 195 samples into non-flooded classes. Simultaneously, in run-3, the MVODTL-FD technique categorized 188 pieces into flooded classes and 196 pieces into non-flooded types. Finally, in run-4, the MVODTL-FD approach categorized 189 pieces into flooded type and 198 pieces into non-flooded type (Table 1).

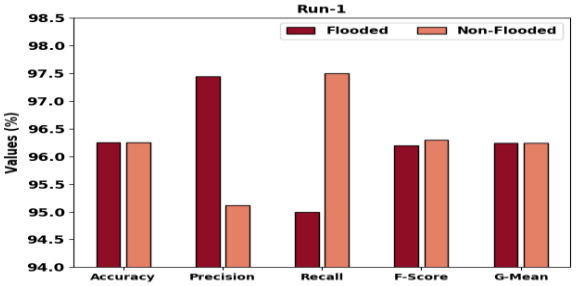

Figure 5. Result analysis of MVODTL-FD approach under run1

Table 1. Provides the overall flood detection results of the MVODTL-FD model under five distinct runs

Class	Accuracy	Precision	Recall	F-Score	G-Mean
			Run-1		
Flooded	96.25	97.44	95.00	96.20	96.24
Non-Flooded	96.25	95.12	97.50	96.30	96.24
Average	96.25	96.28	96.25	96.25	96.24
			Run-2		
Flooded	94.75	97.35	92.00	94.60	94.71
Non-Flooded	94.75	92.42	97.50	94.89	94.71
Average	94.75	94.89	94.75	94.75	94.71
			Run-3		
Flooded	96.00	97.92	94.00	95.92	95.98
Non-Flooded	96.00	94.23	98.00	96.08	95.98
Average	96.00	96.07	96.00	96.00	95.98
			Run-4		
Flooded	96.75	98.95	94.50	96.68	96.72
Non-Flooded	96.75	94.74	99.00	96.82	96.72
Average	96.75	96.84	96.75	96.75	96.72
			Run-5		
Flooded	96.50	97.94	95.00	96.45	96.49
Non-Flooded	96.50	95.15	98.00	96.55	96.49
Average	96.50	96.54	96.50	96.50	96.49

Figure 5 demonstrates the classification results of the MVODTL-FD model under run-1. The MVODTL-FD model has identified flooded samples with $accu_y$ of 96.25%, $prec_n$ of 97.44%, $reca_l$ of 95%, F_{score} of 96.20%, and G_{mean} of 96.24%. Besides, the MVODTL-FD model has identified non-flooded samples with $accu_y$ of 96.25%, $prec_n$ of 95.12%, $reca_l$ of 97.50%, F_{score} of 96.30%, and G_{mean} of 96.24%. Moreover, the MVODTL-FD model has attained an average $accu_y$ of 96.25%, $prec_n$ of 96.28%, $reca_l$ of 96.25%, F_{score} of 96.25%, and G_{mean} of 96.24%.

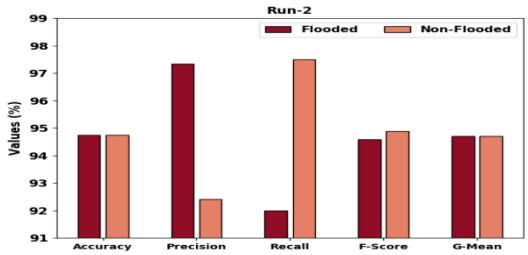

Figure 6. Result analysis of MVODTL-FD approach under run2

Figure 6 establishes the classification results of the MVODTL-FD technique under run-2. The MVODTL-FD algorithm has identified flooded samples with $accu_y$ of 94.75%, $prec_n$ of 97.35%, $reca_l$ of 92%, F_{score} of 94.60%, and G_{mean} of 94.71%. Moreover, the MVODTL-FD method has identified non-flooded samples with $accu_y$ of 94.75%, $prec_n$ of 92.42%, $reca_l$ of 97.50%, F_{score} of 94.89%, and G_{mean} of 94.71%. The MVODTL-FD approach has gained an average $accu_y$ of 94.75%, $prec_n$ of 94.89%, $reca_l$ of 94.75%, F_{score} of 94.75%, and G_{mean} of 94.71%.

Figure 7 illustrates the classification results of the MVODTL-FD method under run-3. The MVODTL-FD technique has identified flooded samples with $accu_y$ of 96%, $prec_n$ of 97.92%, $reca_l$ of 94%, F_{score} of 95.92%, and G_{mean} of 95.98%. As well, the MVODTL-FD algorithm has identified non-flooded samples with $accu_y$ of 96%, $prec_n$ of 94.23%, $reca_l$ of 98%, F_{score} of 96.08%, and G_{mean} of 95.98%. Likewise, the MVODTL-FD method has gained an average $accu_y$ of 96%, $prec_n$ of 96.07%, $reca_l$ of 96%, F_{score} of 96%, and G_{mean} of 95.98%.

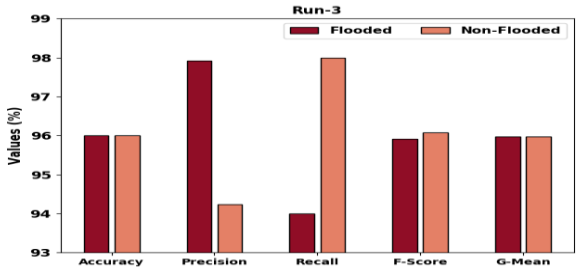

Figure 7. Result analysis of MVODTL-FD approach under run3

Figure 8 reveals the classification results of the MVODTL-FD method under run-4. The MVODTL-FD approach has identified flooded samples with $accu_y$ of 96.75%, $prec_n$ of 98.95%, $reca_l$ of 94.50%, F_{score} of 96.68%, and G_{mean} of 96.72%. In addition, the MVODTL-FD method has identified non-flooded samples with $accu_y$ of 96.75%, $prec_n$ of 94.74%, $reca_l$ of 99%, F_{score} of 96.82%, and G_{mean} of 96.72%. Additionally, the MVODTL-FD approach has reached an average $accu_y$ of 96.75%, $prec_n$ of 96.84%, $reca_l$ of 96.75%, F_{score} of 96.75%, and G_{mean} of 96.72%.

Figure 9 portrays the classification results of the MVODTL-FD method under run-5. The MVODTL-FD approach has identified flooded samples with $accu_y$ of 96.50%, $prec_n$ of 97.94%, $reca_l$ of 95%, F_{score} of 96.45%, and G_{mean} of 96.49%. Moreover, the MVODTL-FD algorithm has identified non-flooded samples with $accu_y$ of 96.50%, $prec_n$ of 95.15%, $reca_l$ of 98%, F_{score} of 96.55%, and G_{mean} of 96.49%. In addition, the MVODTL-FD method has reached

an average $accu_y$ of 96.50%, $prec_n$ of 96.54%, $reca_l$ of 96.50%, F_{score} of 96.50%, and G_{mean} of 96.49%.

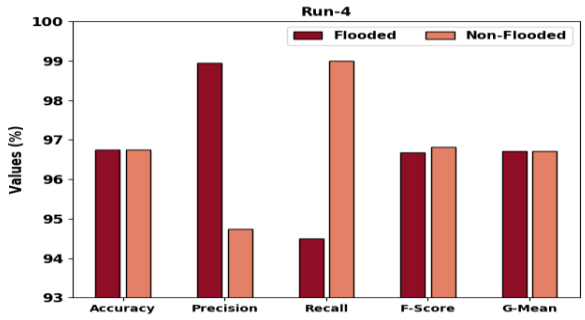

Figure 8. Result analysis of MVODTL-FD approach under run4

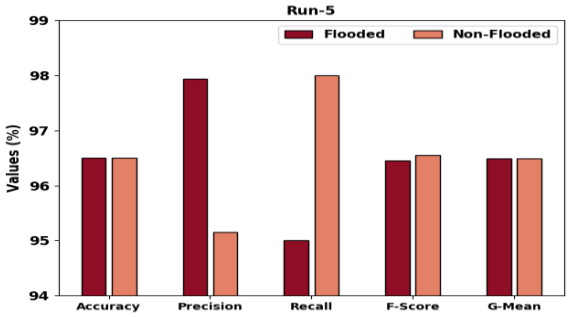

Figure 9. Result analysis of MVODTL-FD approach under run5

The training accuracy (TRA) and validation accuracy (VLA) acquired by the MVODTL-FD approach under the test dataset is exemplified in Figure 10. The experimental outcome implicit MVODTL-FD algorithm has gained maximal values of TRA and VLA. Seemingly, the VLA is greater than TRA.

Figure 10. TRA and VLA analysis of MVODTL-FD approach

The training loss (TRL) and validation loss (VLL) obtained by the MVODTL-FD technique in the test dataset are displayed in Figure 11. The experimental outcome denotes the MVODTL-FD approach has exhibited the least values of TRL and VLL. Specifically, the VLL is lesser than TRL.

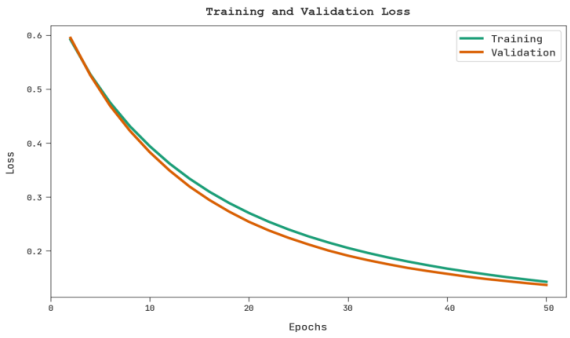

Figure 11. TRL and VLL analysis of MVODTL-FD approach

A transparent precision-recall investigation of the MVODTL-FD approach in the test dataset is described in Figure. 12. The figure denoted the MVODTL-FD algorithm has resulted in enhanced precision recall values under all classes.

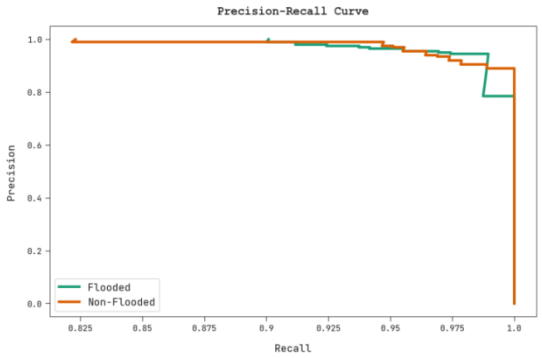

Figure 12. Precision-recall analysis of MVODTL-FD approach

A brief ROC study of the MVODTL-FD approach under the test dataset is portrayed in Figure 13. The results denoted the MVODTL-FD algorithm has displayed its capability in classifying different class labels in the test dataset.

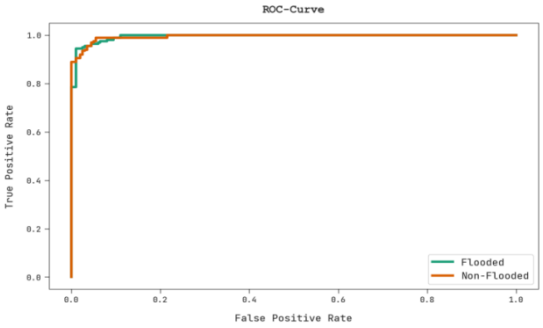

Figure 13. ROC curve analysis of MVODTL-FD approach

Finally, a detailed comparative $accu_y$ examination of the MVODTL-FD model with recent models is made in Figure 14. The experimental values infer that the SMVD-CNN, RF, AHP, and SVM models have reached lower $accu_y$ values of 84.55%, 86.94%, 84.47%, and 85.43% respectively. The CNN-LE model has obtained a slightly improved $accu_y$ of 90.47%. Then, the DNN model reached a reasonable $accu_y$ of 91.55%.

However, the MVODTL-FD model has shown enhanced performance with a maximum $accu_y$ of 96.75%. These results ensured the superior flood detection performance of the MVODTL-FD model.

5. Conclusion

In this study, a new MVODTL-FD technique was developed for the flood detection process. In the demonstrated MVODTL-FD technique, remote sensing images are investigated for the effectual detection of floods. To accomplish this, the demonstrated MVODTL-FD technique utilized GNF based image preprocessing approach to eliminate the noise. In addition, the proposed MVODTL-FD technique uses a deep convolutional neural network-based Squeeze Net model for feature extraction, and the hyperparameter tuning process is performed using the MVO algorithm. At last, the flood detection process is performed using the SVM classifier. To demonstrate the

enhanced version of the MVODTL-FD model, a wide-ranging experimental analysis is performed. The comparison study reported the better version of the MVODTL-FD model over other DL models. In the future, the performance of the MVODTL-FD model was extended to utilize hybrid DL models for enhanced detection efficiency at real-time.

Funding statement

No funding was received for this study.

Acknowledgment

The authors would like to thank the Holycross Engineering College, SRM Institute of Science and Technology, Vel Tech Multi Tech Dr.Rangarajan Dr.Sakunthala Engineering College, and Chennai Institute of Technology for providing the resources.

Data availability statement

Available Based on Request. The datasets generated and or analyzed during the current study are not publicly available due to the extension of the submitted research work. They are available from the corresponding author upon reasonable request.

Conflict of Interest

The authors declare they have no conflicts of interest to report regarding the present study.

References

Ahmad K., Pogorelov K., Riegler M., Ostroukhova O. and Halvorsen P. (2019). Automatic detection of passable roads after floods in remote sensed and social media data, *Signal Processing: Image Communication,* **74**, 110–118.

Akshaya K.G. and Sathyanarayan R.S. (2023). Prediction of Land Use and Landcover Changes in Tiruppur Tamilnadu Using Hybrid Convolutional Neural Network. *Global NEST Journal*, **25**, 1-11.

Bhadra T., Chouhan A., Chutia D., Bhowmick A. and Raju P.L.N. (2020). Flood detection using multispectral images and SAR data, in Proc. International Conference on Machine Learning, Image Processing, *Network Security and Data Sciences*, Silchar, India, 294–303.

Chawan A.C., Kakade V.K. and Jadhav J.K. (2020). Automatic detection of flood using remote sensing images, *Journal of Information Technology*, **2**, 11–26.

Duhayyim M.A., Alsolai H., Hassine S.B.H., Alzahrani J.S. and Salama A.S. (2023). Automated deep learning driven crop classification on hyperspectral remote sensing images, *Computers, Materials & Continuas,* **74**, 3167–3181.

Hashemi-Beni L. and Gebrehiwot A.A. (2021). Flood extent mapping: An integrated method using deep learning and region growing using UAV optical data, *IEEE Journal of Selected Topics in Applied Earth Observations and Remote Sensing,* **14**, 2127–2135.

Jain P., Schoen-Phelan B. and Ross R. (2020). Automatic flood detection in SentineI-2 images using deep convolutional neural networks, in Proc. 35th Annual ACM Symposium on Applied Computing, Brno, Czech Republic, 617–623.

Jena R., Pradhan B., Beydoun G., Al-Amri A. and Sofyan H. (2020). Seismic hazard and risk assessment: a review of state-of-the-art traditional and GIS models, *Arabian Journal of Geosciences*, **13**, 1–21.

Karthikeyan B., Mohanasundaram R., Suresh P. and Jagan Babu J. (2023). Deep learning and machine learning based air pollution prediction model for smart environment design planning. *Global NEST Journal*, **25**, 11-19.

Katiyar V., Tamkuan N. and Nagai M. (2021). Near-real-time flood mapping using off-the-shelf models with SAR imagery and deep learning, *Remote Sensing*, **13**, 1–23.

Khan A.A., Jamil A., Hussain D., Ali I. and Hameed A.A. (2022). Deep learning-based framework for monitoring of debris-covered glacier from remotely sensed images, *Advances in Space Research*, Online First.

Li J., Meng Y., Li Y., Cui Q. and Yang X. (2022). Accurate water extraction using remote sensing imagery based on normalized difference water index and unsupervised deep learning, *Journal of Hydrology,* **612**, 128202.

Li W., Liu H., Wang Y., Li Z. and Jia Y. (2019). Deep learning-based classification methods for remote sensing images in urban built-up areas, *IEEE Access*, **7**, 36274–36284.

Li X., Liu B., Zheng G., Ren Y. and Zhang S. (2020). Deep-learning-based information mining from ocean remote-sensing imagery, *National Science Review,* **7**, 1584–1605.

Mirjalili S., Mirjalili S.M. and Hatamlou A. (2016). Multi-verse optimizer: a nature-inspired algorithm for global optimization, *Neural Computing and Applications*, **27**, 495–513.

Munawar H.S., Hammad A.W. and Waller S.T. (2022). Remote sensing methods for flood prediction: a review, *Sensors*, **22**, 1–21.

Munawar H.S., Ullah F., Qayyum S. and Heravi A. (2021). Application of deep learning on UAV-based aerial images for flood detection, *Smart Cities*, **4**, 1220–1242.

Rambour C., Audebert N., Koeniguer E., Le B. and Crucianu M. (2020). Flood detection in time series of optical and SAR images, *International Archives of the Photogrammetry, Remote Sensing and Spatial Information Sciences,* **43**, 1343–1346.

Santhanaraj R.K., Rajendran S., Romero C.A.T. and Murugaraj S.S. (2023). Internet of Things Enabled Energy Aware Metaheuristic Clustering for Real Time Disaster Management. *Computer. System. Science. Engineering*., **45**, 1561–1576.

Shafique A., Cao G., Khan Z., Asad M. and Aslam M. (2022). Deep learning-based change detection in remote sensing images: a review, *Remote Sensing*, **14**, 1–40.

Shaiba H., Marzouk R., Nour N. Negm A. Mustafa Hilal. *et al*. (2022). Weather forecasting prediction using ensemble machine learning for big data applications, Computers, Materials & Continua, 73, no. 2, 3367–3382.

Shehata M. and Rashed E.F. (2021). Temporal model for mitigating urban development uncertainty, *Journal of Umm Al-Qura University for Engineering and Architecture*, **12**, 31–38.

Surendran R., Alotaibi Y. and Subahi A.F. (2023). Lens-Oppositional Wild Geese Optimization Based Clustering Scheme for Wireless Sensor Networks Assists Real Time Disaster Management. *Computer. Systems. Science. Engineering* ., **46**, 835–851.

Surendran R., Alotaibi Y. and Subahi A.F. (2023). Wind Speed Prediction Using Chicken Swarm Optimization with Deep Learning Model. *Computer Systems Science & Engineering,* **46**, 3.

Tamilvizhi T., Surendran R., Romero C.A.T. and Sadish M. (2022). Privacy preserving reliable data transmission in cluster based vehicular adhoc networks, *Intelligent Automation & Soft Computing*, **34**, 1265–1279.

Tanim A.H., C.B. McRae H., Tavakol-Davani and Goharian E. (2022). Flood detection in urban areas using satellite imagery and machine learning, *Water,* **14,** 1–20.

Zhang X., Nguyen H., Choi Y., Bui X.N. and Zhou J. (2021). Novel extreme learning machine-multi-verse optimization model for predicting peak particle velocity induced by mine blasting, *Natural Resources Research*, **30**, no. 6, 4735–4751.